ARTICLES

Adsorption of Copolymers in a Selective Nanoslit: A Hybrid Density Functional Theory

Houyang Chen,[†] Jun Cai,[†] Zhencheng Ye,[†] Changjun Peng,[†] Honglai Liu,*[,†] Ying Hu,[†] and Jianwen Jiang*[,‡]

State Key Laboratory of Chemical Engineering and Department of Chemistry, East China University of Science and Technology, Shanghai 200237, China, and Department of Chemical and Biomolecular Engineering, National University of Singapore, Singapore 117576

Received: March 24, 2008; Revised Manuscript Received: May 12, 2008

A hybrid density functional theory (DFT) is developed for adsorption of copolymers in a selective nanoslit. The DFT incorporates a single-chain simulation for the ideal-gas free energy functional with two weighted density approximations for the residual free energy functional. The theory is found to be insensitive to the width parameter used in the weighted density. Theoretical predictions are in excellent agreement with simulation results in the segment density profiles and the adsorption configurations including tail, loop, and train for copolymers with various sequences over a wide range of surface affinity. The bridge conformation is also observed in multiblock copolymers. Ordered assembly is facilitated in copolymers with longer chain/block and at stronger attraction between segment B and the slit wall. While diblock copolymer shows the longest tail, alternating copolymer has the shortest. As the attraction between segment B and the slit wall increases, the average size and fraction decrease for tail, but increase for loop and train.

1. Introduction

Polymer adsorption at interface is of central importance for many practical applications. Because of the geometric restriction and surface interaction, polymer conformation changes upon adsorption. Extensive experimental, theoretical, and simulation studies have been reported to examine the microscopic mechanism and structure for polymer adsorption, as summarized in several review articles.[1–4] As compared to homopolymers, the behavior of copolymers at interface is substantially richer and the understanding is far less complete. Early theoretical models for copolymers were primarily based on the self-consistent-field (SCF) theory[5–9] and Landau expansions.[10,11] The segments profiles, configurations, and surface tensions in both bulk and interfacial phases were investigated. These models could also be used to mimic surfactant, especially nonionic and amphiphilic surfactants.

In recent years, there have been increasingly interests in the use of density functional theory (DFT) for polymeric systems. Chandler et al.[12,13] developed a DFT as a direct extension from the reference-site-interaction model for the simple fluids.[14] On the basis of the generalized van der Waals approximation,[15] Woodward proposed a DFT for polymers.[16] Previous DFTs for copolymer systems, e.g., by Melenkevitz and Muthukumar[17] and McMullen and Freed,[18] were heavily influenced by SCFT and Landau expansions for the formulation of the free energy functional, which results in the insufficiency of the theory describing the segment level behavior of copolymer. Combining a modification of Rosenfeld's fundamental measure theory (FMT)[19] for the excluded-volume effect and a first-order thermodynamic perturbation theory[20] for the chain connectivity, Wu et al.[21,22] proposed a DFT for inhomogeneous mixtures and copolymer of polymeric fluids. Following Yethiraj and Woodward,[23] Cai et al.[24,25] developed the equation-of-state-based DFT for hard-sphere chain mixtures by introducing a partial molecular free energy functional. Ye et al.[26–28] extended it further to both homopolymer mixtures and copolymers with attractive interaction via a new weighted density approximation. The weighted density is usually used to mimic the oscillatory density distribution in an inhomogeneous fluid. Chen et al.[29] used Ye's method to solve the density profiles of polymer confined between two nanopatterned walls. In order to study the structures and morphologies of block copolymer thin films, Frischknecht et al.[30,31] presented a DFT based on the polymer-reference-interaction-site model (PRISM). The free energy minimization of the DFT led to an explicit set of integral equations describing the chain connectivity and coupling between the inhomogeneous density distribution and the unknown effective field. Nath and co-workers[32,33] studied the structures of fluids near patterned surfaces, by using a mathematical scheme that permitted efficient numerical calculation of the relevant two-dimensional density profiles.

As an extension of our previous work,[20] in this work we use the hybrid DFT to study the adsorption of copolymers in a selective nanoslit. The hybrid DFT combines a single-chain Monte Carlo (MC) simulation for the ideal-gas free energy functional with two weighted density approximations developed, respectively, by Yethiraj et al.[23] and by Ye et al.[26] for the residual free energy functional. In our previous work,[26] the single-chain simulation for the intramolecular interaction was approximated by the random flight model. In a selective slit, however, as we shall see that the single-chain simulation turns out to be crucial. To validate the hybrid DFT presented here, MC simulations were also performed. The method for obtaining the microscopic configurations from DFT can be found in our previous work.[26–29,34]

* Corresponding authors. E-mail: (H.L.) hlliu@ecust.edu.cn; (J.J.) chejj@nus.edu.sg.
[†] East China University of Science and Technology.
[‡] National University of Singapore.

10.1021/jp802633p CCC: $40.75
Published on Web 07/23/2008

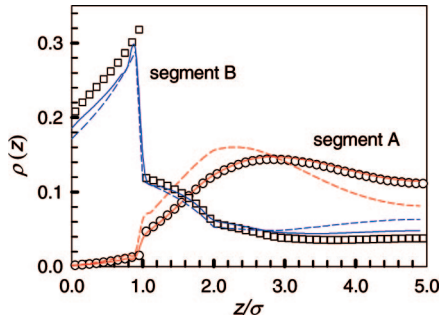

Figure 1. Segment density profiles of copolymer A_8B_8. The reduced surface energies are $\lambda_{AW} = -1.0$ and $\lambda_{BW} = 1.0$. Solid lines, predictions of this work; dashed lines, work of Ye et al.;[28] symbols, simulations.

Following this introduction, we briefly describe our DFT in Section 2. In Section 3, we present the theoretically calculated segment density profiles and compare them with the simulation results. Adsorption configurations, including tail, loop, tail, and bridge are also predicted by our theoretical model and MC simulations. Finally, the conclusions are summarized in Section 4.

2. Theory

2.1. Theoretical Framework. For an inhomogeneous system, the grand potential is

$$\Omega[\rho_M] = F^{id}[\rho_M] + F^{re}[\rho_M] + \int V_{ext}(R)\rho_M(R)dR - \mu \int \rho_M(R)dR \quad (1)$$

where $F^{id}[\rho_M]$ and $F^{re}[\rho_M]$ are the intrinsic Helmholtz free energy functions for ideal gas and the residual contributions, respectively; μ and V_{ext} are chemical potential and external field, respectively.

Similar to Yethiraj's[35] and our previous work,[26] $F^{re}[\rho_M]$ can be decomposed into

$$F^{re} = F^{re}_{hs} + F^{re}_{attr} \quad (2)$$

Here the subscript "hs" means hard sphere, and the subscript "attr" denotes attractive contribution. The following weighted density approximations are adopted

$$F^{re}_{hs}[\rho_M] = \sum_{i=1}^{H} \int \rho_i(r) f^{(i)}_{hs}[\bar{\rho}^{(i)}_{hs}(r)]dr \quad (3a)$$

$$F^{re}_{attr}[\rho_M] = \sum_{i=1}^{H} \int \rho_i(r) f^{(i)}_{attr}[\bar{\rho}^{(i)}_{attr}(r)]dr \quad (3b)$$

where H is the total number of segment types. $f^{(i)}_{hs}[\bar{\rho}]$ is the partial molecular residual free energy functional of hard-sphere segment i at a given weighted density profile $\bar{\rho}^{(i)}_{hs}(r)$ responsible for the excluded-volume effect. $f^{(i)}_{attr}(\bar{\rho})$ is the difference between the partial molecular residual free energy functional for square-well chains and that for hard-sphere chains. The expressions of $f^{(i)}_{hs}$ and $f^{(i)}_{attr}$ have been given previously. $\bar{\rho}(r)$ is the weighted density given as

$$\bar{\rho}(r) = \int w(|r' - r'|)\rho(r')dr' \quad (4)$$

For hard-sphere contribution, $w^i_{hs}(r) = 3\Theta(\sigma_i - r)/4\pi\sigma_i^3$. For attractive contribution, the corresponding weighted function can be chosen as $w^i_{attr}(r) = 3\Theta(L_w\,\sigma_i - r)/4\pi(L_w\,\sigma_i)^3$. Unless otherwise mentioned, the width parameter L_w is set at 1.5 in this study. However, the effect of L_w on the prediction of density profile is examined.

At equilibrium, Ω is an extremum with respect to the change in density distribution, i.e.,

$$\delta\Omega/\delta\rho_M(R) = 0 \quad (5)$$

Thus, we obtain the density profile of molecules,

$$\rho_M(R) = \exp\left[\beta\mu_M - \beta U_M(R) - \beta V_M(R) - \frac{\delta F^{re}[\rho_M]}{\delta\rho_M(R)}\right] \quad (6)$$

where $\beta = 1/kT$. k is the Boltzmann factor and T the absolute temperature. It is convenient to define the chain segment density

$$\rho_h(r) = \int \sum_{j=1}^{m} \delta^*_{h,j}\rho_M(R)\delta(r - r_j)dR, \qquad h = 1, 2, \cdots, H \quad (7)$$

where ρ_h is the segment density profile of kind h, and m is the chain length of copolymer, r is the coordinate of segment. If the kind of jth segment in the copolymer molecule is h, $\delta^*_{h,j} = 1$; otherwise, $\delta^*_{h,j} = 0$.

Similar to homopolymer,[27] for copolymer we have

$$\rho_h(r) = \int \sum_{j=1}^{m} \delta^*_{h,j}\delta(r - r')\exp[\beta\mu_M - \beta U_M - \beta V_M - \sum_{i=1}^{m}\sum_{s=1}^{H} \delta^*_{s,i}\lambda_s(r_i)]dR \quad (8)$$

where

$$\lambda_{hs}(r) = \beta f_{hs}[\bar{\rho}_{hs}(r)] + \int \rho(r')w_{hs}(|r' - r|)\frac{\partial\beta f_{hs}[\bar{\rho}_{hs}(r)]}{\partial\bar{\rho}_{hs}(r')}dr' \quad (9a)$$

$$\lambda_{attr}(r) = \beta f_{attr}[\bar{\rho}_{attr}(r)] + \int \rho(r')w_{attr}(|r' - r|)\frac{\partial\beta f_{attr}[\bar{\rho}_{attr}(r)]}{\partial\bar{\rho}_{attr}(r')}dr' \quad (9b)$$

We can adopt eq 8 to solve the segment density profiles. It requires a single chain simulation for intramolecular interaction $V_{M,h}$. The density profiles is calculated from

$$\rho_h(r) = \exp(\beta\mu_{M,h})\left\langle \int \sum_{j=1}^{m_h} \delta(r - r')\exp\left[-\beta U_{M,h} - \sum_{i=1}^{m_h}\lambda_h(r_i)\right]dR_h \right\rangle \quad (10)$$

where $\langle \cdots \rangle$ is the ensemble average of a single chain. Starting with an initial guess, the density profile was calculated using eqs 9–10 and a single-chain simulation. The procedure was iterated until approaching a desired accuracy. The number of iteration depends on system and generally a larger iterative number is required for a system with stronger polymer-slit interaction. In most of our systems, the iterative number was less than 60. The calculation took about 6 min in an Intel XEON 1.6 G DUAL CORE processor.

Multichain MC simulations were also performed in a canonical ensemble with a box of $L_x \times L_y \times L_z = 16.4\sigma \times 16.4\sigma \times 10\sigma$. The periodic boundary conditions were adopted in the x and y directions, while in the z direction two identical impenetrable surfaces. Two types of trial moves, namely,

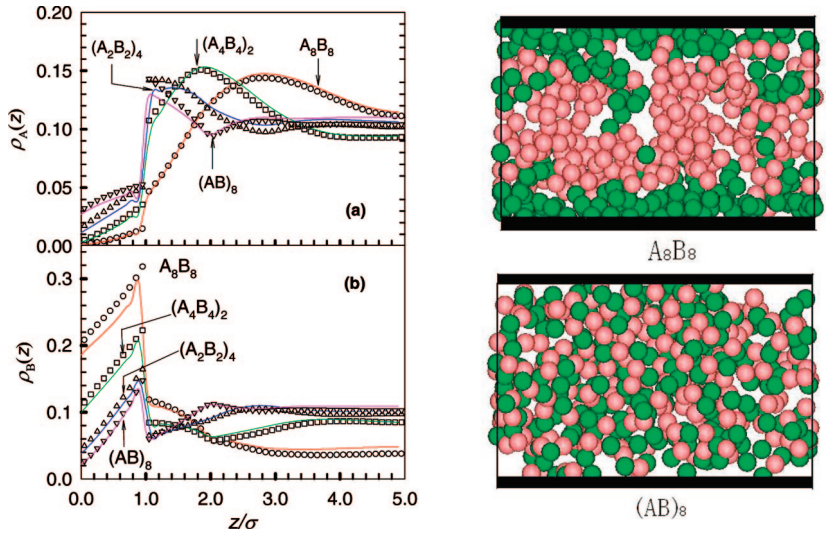

Figure 2. Segment density profiles of copolymers with different sequences. (a) Segment A and (b) segment B. The reduced surface energies are $\lambda_{AW} = -1.0$ and $\lambda_{BW} = 1.0$. Solid lines, predictions; symbols, simulations. On the right are the simulation snapshots for A_8B_8 and $(AB)_8$; pink, segment A; green, segment B.

translation and jiggling,[36] were adopted in both the single chain and the multichain simulations. In the first trial move, a randomly selected chain is translated with a random displacement in the x, y, or z direction. In jiggling, each bond is subject to a rotation. The new bond vector is calculated by rotating the old one in an arbitrary solid angle. In each simulation, we used about 10^6 steps for equilibrium and 10^7 steps to calculate the ensemble averages.

2.2. Molecular Model. The copolymers are modeled as square-well chains with SW interaction potential between segments

$$u(r_{ij}) = \begin{cases} 0 & r_{ij} > L_{sw}\sigma \\ -\varepsilon_{ij} & \sigma < r_{ij} < L_{sw}\sigma \\ \infty & r_{ij} < \sigma \end{cases} \quad (11)$$

where r_{ij} is the distance between two segments. The SW potential width L_{sw} is fixed at 1.5 in this study.

The interaction between a segment and the slit wall is also represented by SW potential

$$u(r_{i-\text{wall}}) = \begin{cases} 0 & r_{i-\text{wall}} > \sigma \\ -\lambda_{i-W} & 0 < r_{i-\text{wall}} < \sigma \\ \infty & r_{i-\text{wall}} < 0 \end{cases} \quad (12)$$

where r_{i-W} is the distance between the center of segment and the wall.

The equation-of-state for hard-sphere chain (hsc) fluid developed by Hu et al. is used to calculate the residual free energy of the repulsive part.[37] The SAFT-VR equation-of-state for the square-well chain (swc) fluid developed by Gil-Villegas et al. is used to calculate the residual free energy of the attractive part.[38]

Throughout this work, a negative energy means repulsion and a positive sign for attraction. The interactions between all polymer segments are assumed to be attractive. Except Figure 3, all copolymers $(A_xB_x)_{8/x}$ considered consist of 16 SW segments but with various sequences by varying x. The slit wall attracts B segments but repels A segments. In MC simulations, the average packing fraction of copolymers inside the slit is fixed at $\eta = (\pi/6)\bar{\rho}\sigma^3 = 0.1$ and the slit width is $H = 10\sigma$. For comparison with simulation data, the predictions from DFT are calculated at the same packing fractions. The reduced temperature is taken as $T^* = kT/\varepsilon_{AA} = 6.0$. The energy parameters are given by $\varepsilon_{BB}/\varepsilon_{AA} = 0.5$ and $\varepsilon_{AB} = \sqrt{\varepsilon_{AA}\varepsilon_{BB}}$.

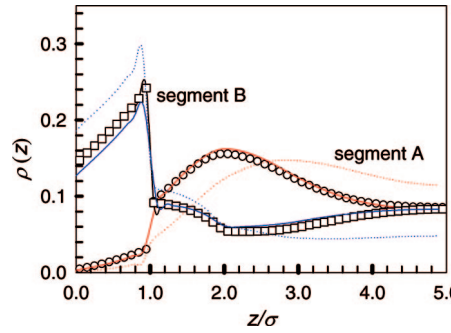

Figure 3. Segment density profiles of copolymer A_4B_4. The reduced surface energies are $\lambda_{AW} = -1.0$ and $\lambda_{BW} = 1.0$. Solid lines: predictions and symbols: simulations. For comparison, theoretical predictions for A_8B_8(dotted lines) are also included.

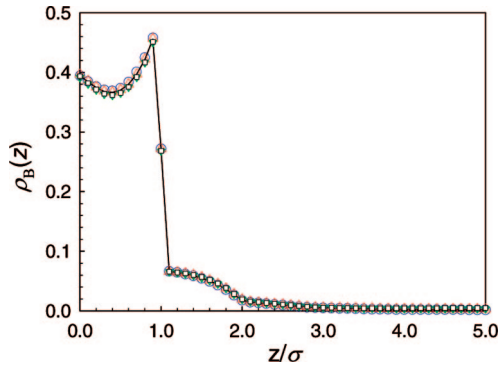

Figure 4. Segment B density profiles of copolymer A_8B_8 with different L_w in the weighted function. The reduced surface energies are $\lambda_{AW} = -1.0$ and $\lambda_{BW} = 2.0$. Solid lines, predictions with $L_w = 1.5$; symbols, simulations. Circles, $L_w = 1.2$; upward triangles, $L_w = 1.8$; downward triangles, $L_w = 2.0$; squares, $L_w = 2.5$.

3. Results and Discussion

3.1. Density Profiles. Figure 1 shows the comparison between the theoretical predictions of this work and those of Ye et al.,[28] as well as the simulation results for the segment density profiles of copolymer A_8B_8 in a selective slit at $\lambda_{AW} =$

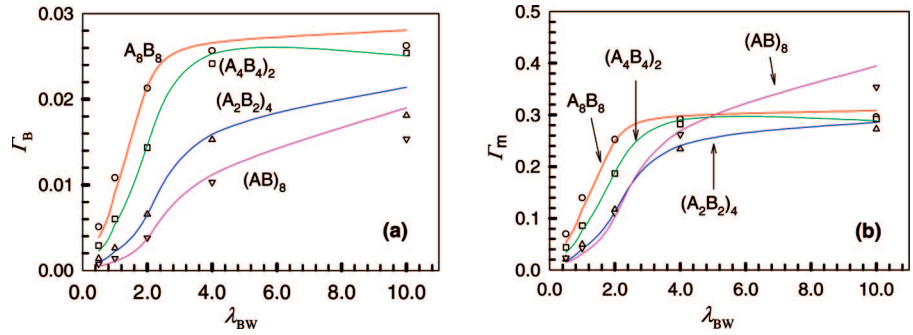

Figure 5. Adsorption ratio of (a) segment B and (b) copolymers with different sequences as a function of λ_{BW}. The reduced surface energy $\lambda_{AW} = -1.0$. Downward triangles, $(AB)_8$; upward triangles, $(A_2B_2)_4$; squares, $(A_4B_4)_2$; circles, A_8B_8; lines, predictions; symbols, simulations.

-1.0 and $\lambda_{BW} = 1.0$. For attractive segments B, the density increases near the slit wall up to a maximum and then drops sharply at $z = \sigma$. In contrast, the density of repulsive segments A is vanishingly zero close to the wall and rises upon moving away from the wall. This is a counterbalance between the chain connectivity and the attractive/repulsive interactions with the wall. The predictions of this work are in prefect agreement with the simulation and superior to Ye et al. For copolymer in a nonselective slit, the results of Ye et al. agree with simulation. Nevertheless, it deviates from simulation in a selective slit. The main reason is that single-chain simulation used in this work is more accurate for the intrachain interactions than the random-flight model.

Figure 2 shows the segment density profiles of copolymers with different sequences A_8B_8 and $(AB)_8$ in a selective slit at $\lambda_{AW} = -1.0$ and $\lambda_{BW} = 1.0$. The theoretical predictions catch the main characteristics of the simulation results. The repulsive segments A show a depletion layer near the wall and due to the chain connectivity a peak is observed. The exact position of the peak depends largely on the length of block A; as the length increases, the peak moves away from the wall. Interestingly, there appears a minimum in the density profile of $(AB)_8$ due to the packing effect. The attractive segments B show an adsorption layer near the wall. As expected, the density of segments B with attraction near the wall is constantly larger than that of segments A. The discontinuity in the SW potential causes a discontinuity in the density profile at $z = \sigma$. Similar behavior has been observed in a selective slit[22] and other monomeric SW fluids near a SW wall.[39,40]

The ordered assembly of the same type of segments is observed in Figure 2. At a fixed chain length, the assembly becomes more disordered as the length of block decreases. This is consistent with experimental study of Velankar et al., in which the degree of ordered assembly increases with increasing block length.[41] Figure 2 also show that the ordered assembly of diblock copolymer is easier to form than alternating copolymer, as visualized by the two simulation snapshots. The domains of segments A and B of A_8B_8 diblock polymer are richer and clearer than those of $(AB)_8$ alternating polymer. Compared to diblock copolymer, alternating copolymer prefers to a more coiled structure. In other words, a copolymer possesses the characteristics of a homopolymer as the length of block decreases. This was also observed by Ye et al.[28] in a off-lattice model and by Sun et al.[42] in a lattice model.

The effect of chain length on the segment density profiles is shown in Figure 3. With decreasing chain length (from A_8B_8 to A_4B_4), the density of segments B near the slit wall decreases, while that of segments A increases. The ordered assembly of A_8B_8 is more obvious than A_4B_4, which was also found in previous studies.[43–45] This is mainly because the driving force

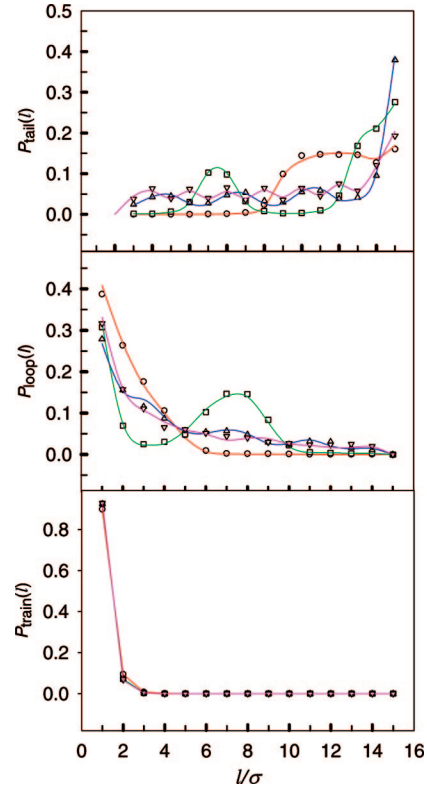

Figure 6. Distribution probabilities of tail, loop and train versus length for copolymer with different sequences. Circles, A_8B_8; squares, $(A_4B_4)_2$; upward triangles, $(A_2B_2)_4$; downward triangles, $(AB)_8$. The reduced surface energies are $\lambda_{AW} = -1.0$ and $\lambda_{BW} = 1.0$. Solid lines, predictions; symbols, simulations.

for assembly is greater for longer copolymer.[45] Particularly, no phase separation occurs in the bulk phase for A_4B_4, i.e., there exists a larger number of free chains. This indicates the system of shorter copolymer in the slit is more homogeneous beyond a distance $z/\sigma \approx 4.3$. The distance becomes larger as the chain length increases. When z/σ is greater than half of the slit width, the behavior disappears in the center of the slit. This phenomenon was also found by Cao and Wu,[22] in which the van der Waals approximation was adopted for the attractive part of the free energy. However, the van der Waals approximation does not accurately describe the particle−particle and the intramolecular long-range correlations.[28] Upon comparison, the results of this work show better agreement with simulation results.

The effect of the width parameter L_w in the weighted function is examined. Figure 4 shows segment B density profiles of copolymer A_8B_8 with different L_w in a selective slit at $\lambda_{AW} = -1.0$ and $\lambda_{BW} = 2.0$. No discernible difference is observed in the density profile by varying L_w from 1.2 to 2.5. This reveals

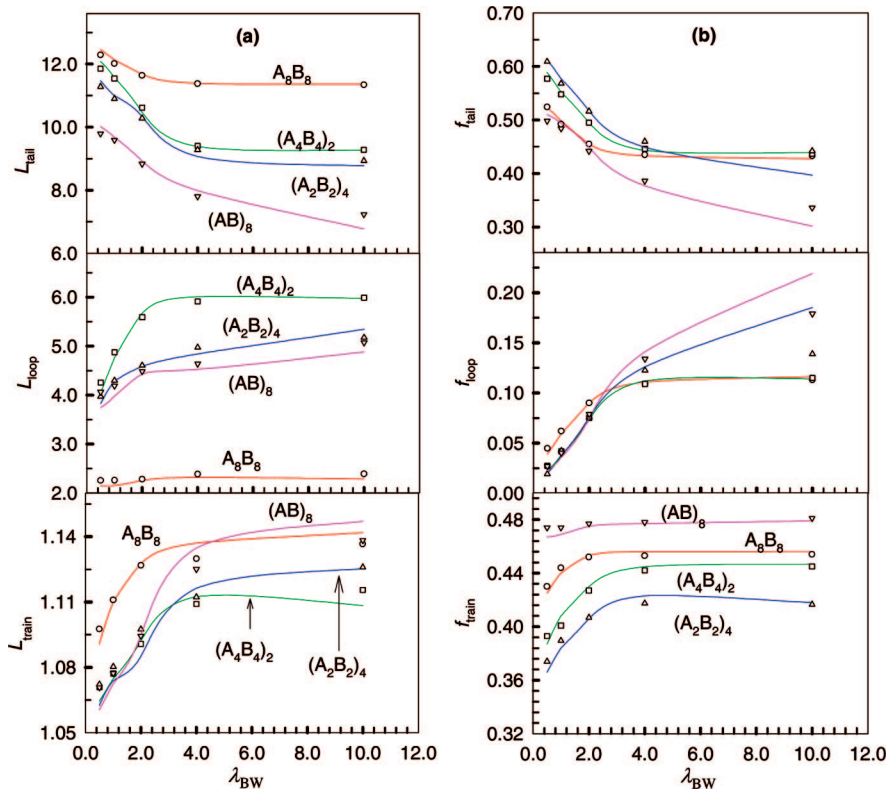

Figure 7. (a) Average sizes and (b) fractions of tail, loop, and train of copolymers with different sequences as a function of λ_{BW}. The reduced surface energy $\lambda_{AW} = -1.0$. Downward triangles, $(AB)_8$; upward triangles, $(A_2B_2)_4$; squares, $(A_4B_4)_2$; circles, A_8B_8; lines, predictions; symbols, simulations.

that the theory is not sensitive to the parameter L_w in the weighted function.

3.2. Adsorption Ratios. Figure 5 shows the adsorption ratio Γ_B of segments B and Γ_m of molecules for copolymer as a function of λ_{BW}. Γ_B refers to the number of adsorbed segments B over the number of all segments (both adsorbed and nonadsorbed). Γ_m is the ratio of adsorbed chains over all polymers in the system. As λ_{BW} increases, both Γ_B and Γ_m initially increase shapely and then reach plateau. It is clear that the attractive interaction with the slit wall plays a key role at low λ_{BW}, while the exclude-volume effect dominates at high λ_{BW}. The theoretical predictions are in good agreement with simulation data in a wider range of λ_{BW}. If λ_{BW} is significantly high (e.g., 10.0), however, the predictions exhibit large deviation from simulations. In this condition, the adsorption of polymer tends to be irreversible and resembles a chemical adsorption. This implies that the hybrid DFT needs to be improved at the strongly nonlinear regime.

At a given λ_{BW}, Γ_B decreases with increasing number of blocks in a copolymer. The greater number of the blocks, the stronger is the effect of chain connectivity, the weaker is the exclude-volume effect, and the behavior of copolymer is closer to alternating copolymer[28] or random copolymer.[42] In the study by Ye et al.,[28] alternating copolymer was demonstrated to resemble homopolymer with effective segment size and effective segment−segment/segment−wall interactions. In lattice simulations,[42] random copolymer was found to behave quantitatively as homopolymer regardless of composition and surface affinity. This intriguing phenomenon also appears in density profiles mentioned above.

At low λ_{BW}, Γ_m increases as the block length of block B increases. At high λ_{BW}, however, the dependence on block length is not monotonic. For short-block copolymers $(A_2B_2)_4$ and $(AB)_8$, Γ_m increases; for long-block copolymers A_8B_8 and $(A_4B_4)_2$, it is nearly a constant. With rapid increase in the adsorption amount of copolymer, the surface becomes crowded. As a result, the adsorbed chains tend to adopt a brushy conformation to facilitate further adsorption at low λ_{BW}.[46] At high λ_{BW}, there are a large number of adsorption sites on the wall and the excluded-volume effect governs the adsorption. A short-block copolymer has more adsorption sites and the probability of adsorption is thus enhanced.

3.3. Adsorption Configurations. Adsorption configurations play a vital role in polymer adsorption and different configurations including tail, loop, train, and bridge behave differently. A sequence of successive segments are referred to as tail if they start from the head or the end of a chain to the first segment in contact with surface; they are referred to as loop if they are between two nearest segments that are in contact with surface; and they are referred to as train if a sequence of successive segments are in contact with the surface. Consequently, the lengths of tail, loop, and train are in the range between 1 and $N - 1$, $N - 2$, and N, respectively.[29,47,48] Bridge refers to a chain that is in contact with both surfaces.

Figure 6 shows the probability distributions of tail, loop and train versus length for copolymers on a selective surface with $\lambda_{BW} = 1.0$. Generally, a high probability for long tail, short loop, and short train is observed. With two completely opposite blocks, the tail of A_8B_8 consists mainly of the repulsive block A_8 and a small portion of segments B due to the chain connectivity. For alternating copolymer $(AB)_8$, the tail length periodically fluctuates. Because of the consecutive sequence of segments, alternating copolymer zips onto the surface.[49] To a certain extent, the adsorption of alternating copolymer is similar to that of homopolymer.[27] For $(A_4B_4)_2$, the block length is between the diblock and alternating copolymers, the tail length

is around 6 and 12. There is a competition between attractive interaction (segments B and wall) and the repulsive interaction (segments A and wall). If the attractive interaction dominates, shorter tails are formed, and vice versa.

Figure 7 shows the average sizes and fractions of tail, loop and train for copolymers with different sequences as a function of λ_{BW}. It is clear that the predicted and simulated results are in quantitative agreement. As the attractive interaction λ_{BW} between segments B and wall increases, more segments B are adsorbed on the wall and form more loops and trains. Consequently, the average size and fraction of tail decrease, while those of loop and train increase. Bridge configuration is also observed in some multiblock copolymers despite very low fraction. Compared to homopolymer, multiblock copolymer is more coiled. Nevertheless, multiblock copolymer can be adsorbed on two different surfaces at high affinity with surface. At a given λ_{BW}, the average size of copolymer decreases as the number of blocks increases. For short-block copolymer, the adsorbing sites are dispersed, the length of repulsive block is reduced and the repulsion decreases. As a result, more repulsive blocks between two adsorbing blocks facilitate the formation of loops.

4. Conclusions

A hybrid density functional theory combining a single-chain Monte Carlo simulation for the ideal-gas free energy functional with two weighted functions for residual part is extended to investigate the adsorption of copolymers in a selective nanoslit. The single-chain simulation is crucial for the selective slit; while for the nonselective slit, it can be approximately by the random flight model. This theory is accurate in a wide range of attractive strength for the predictions of density profiles, adsorption amounts and configurations; although improvement is needed at significantly strong surface affinity. Theoretical prediction is not sensitive to the width parameter in the weighted function. The effects of surface energy, copolymer sequence and chain length on the microscopic segregation of two types of segments are investigated. It is found that longer block and stronger attraction promote ordered assembly. In addition, a critical value of phase separation in the center of slit is estimated. Diblock copolymer possesses the longest tail while alternating copolymer has the shortest. With increasing attraction between segments B and wall, the average size and fraction of tail decrease, while those of loop and train increase.

Acknowledgment. This work is supported by the National Natural Science Foundation of China (Project Nos. 20736002, 20676030), the Doctoral Research Foundation sponsored by the Ministry of Education of China (No. 20050251004), Program for Changjiang Scholars and Innovative Research Team in University (No. IRT0721), the 111 Project (No. B08021), Postdoctoral Foundation of China (H200-9-37), and National University of Singapore.

References and Notes

(1) Dabrowski, A. *Adv. Colloid Interf. Sci.* **2001**, *93*, 135.
(2) Kruk, M.; Jaroniec, M. *Chem. Mater.* **2001**, *13*, 3169.
(3) Ho, Y.-S. *J. Hazardous Mater.* **2006**, *136*, 681.
(4) Ruardy, T. G.; Schakenraad, J. M.; van der Mei, H. C.; Busscher, H. J. *Surf. Sci. Rep.* **1997**, *29*, 3.
(5) Helfand, E. *Acc. Chem. Res.* **1975**, *8*, 295.
(6) Schmid, F. *J. Chem. Phys.* **1996**, *104*, 9191.
(7) Evers, O. A.; Scheutjens, J. M. H. M.; Fleer, G. J. *Macromolecules* **1990**, *23*, 5221.
(8) Petera, D.; Muthukumar, M. *J. Chem. Phys.* **1998**, *109*, 5101.
(9) Pickett, G. T.; Balazs, A. C. *Macromolecules* **1997**, *30*, 3097.
(10) Leibler, L. *Macromolecules* **1980**, *13*, 1602.
(11) Fredrickson, G. H. *Macromolecules* **1987**, *20*, 2535.
(12) Chandler, D.; McCoy, J. D.; Singer, S. J. *J. Chem. Phys.* **1986**, *85*, 5971.
(13) Chandler, D.; McCoy, J. D.; Singer, S. J. *J. Chem. Phys.* **1986**, *85*, 5977.
(14) Ladanyi, B. M.; Chandler, D. *J. Chem. Phys.* **1975**, *62*, 4308.
(15) Freasier, B. C.; Woodward, C. E.; Nordholm, S. *J. Chem. Phys.* **1989**, *90*, 5657.
(16) Woodward, C. E. *J. Chem. Phys.* **1991**, *94*, 3183.
(17) Melenkevitz, J.; Muthukumar, M. *Macromolecules* **1991**, *24*, 4199.
(18) McMullen, W. E.; Freed, K. F. *J. Chem. Phys.* **1990**, *93*, 9130.
(19) Rosenfeld, Y. *Phys. Rev. Lett.* **1989**, *63*, 980.
(20) Wertheim, M. S. *J. Chem. Phys.* **1987**, *87*, 7323.
(21) Yu, Y.-X.; Wu, J. *J. Chem. Phys.* **2002**, *117*, 2368.
(22) Cao, D.; Wu, J. *Macromolecules* **2005**, *38*, 971.
(23) Yethiraj, A.; Woodward, C. E. *J. Chem. Phys.* **1995**, *102*, 5499.
(24) Cai, J.; Liu, H.; Hu, Y. *Fluid Phase Equilib.* **2002**, *194−197*, 281.
(25) Zhang, S.; Cai, J.; Liu, H.; Hu, Y. *Mol. Simul.* **2004**, *30*, 143.
(26) Ye, Z.; Cai, J.; Liu, H.; Hu, Y. *J. Chem. Phys.* **2005**, *123*, 194902.
(27) Ye, Z.; Chen, H.; Cai, J.; Liu, H.; Hu, Y. *J. Chem. Phys.* **2006**, *125*, 124705.
(28) Ye, Z.; Chen, H.; Liu, H.; Hu, Y.; Jiang, J. *J. Chem. Phys.* **2007**, *126*, 134903.
(29) Chen, H.; Ye, Z.; Peng, C.; Liu, H.; Hu, Y. *J. Chem. Phys.* **2006**, *125*, 204708.
(30) Frischknecht, A. L.; Weinhold, J. D.; Salinger, A. G.; Curro, J. G.; Douglas Frink, L. J.; McCoy, J. D. *J. Chem. Phys.* **2002**, *117*, 10385.
(31) Frischknecht, A. L.; Curro, J. G.; Douglas Frink, L. J. *J. Chem. Phys.* **2002**, *117*, 10398.
(32) Nath, S. K.; McCoy, J. D *J. Chem. Phys.* **1997**, *106*, 1950.
(33) Nath, S. K.; Nealey, P. F.; de Pablo, J. J. *J. Chem. Phys.* **1999**, *110*, 7483.
(34) Chen, H.; Ye, Z.; Cai, J.; Liu, H.; Hu, Y.; Jiang, J. *J. Phys. Chem. B* **2007**, *111*, 5927.
(35) Patra, C. N.; Yethiraj, A. *J. Chem. Phys.* **2000**, *112*, 1579.
(36) Dickman, R.; Hall, C. K. *J. Chem. Phys.* **1988**, *89*, 3168.
(37) Hu, Y.; Liu, H.; Prausnitz, J. M. *J. Chem. Phys.* **1996**, *104*, 396.
(38) Gil-Villegas, A.; Galindo, A. *J. Chem. Phys.* **1997**, *106*, 4168.
(39) Zhou, S. *J. Phys. Chem. B* **2003**, *107*, 3585.
(40) Henderson, J. R.; van Swol, F. *J. Chem. Phys.* **1988**, *89*, 5010.
(41) Velankar, S.; Cooper, S. L. *Macromolecules* **1998**, *31*, 9181.
(42) Sun, L.; Peng, C.; Liu, H.; Hu, Y.; Jiang, J. *J. Chem. Phys.* **2007**, *126*, 094905.
(43) Lippa, K. A.; Sander, L. C.; Mountain, R. D. *Anal. Chem.* **2005**, *77*, 7862.
(44) Floriano, M. A.; Firetto, V.; Panagiotopoulos, A. Z. *Macromolecules* **2005**, *38*, 2475.
(45) Zheng, W. Y.; Hammond, P. T. *Macromolecules* **1998**, *31*, 711.
(46) Chen, T.; Liu, H.; Hu, Y. *J. Chem. Phys.* **2001**, 114, 5937.
(47) Chen, H.; Peng, C.; Ye, Z.; Liu, H.; Hu, Y.; Jiang, J. *Langmuir* **2007**, *23*, 2430.
(48) Chen, H.; Peng, C.; Sun, L.; Liu, H.; Hu, Y.; Jiang, J. *Langmuir* **2007**, *23*, 11112.
(49) Ponomarev, A. L.; Sewell, T. D.; Durning, C. J. *Macromolecules* **2000**, *33*, 2662.

JP802633P